Bioorganic & Medicinal Chemistry 22 (2014) 1809–1820

Contents lists available at ScienceDirect

Bioorganic & Medicinal Chemistry

journal homepage: www.elsevier.com/locate/bmc

Polyphenols bearing cinnamaldehyde scaffold showing cell growth inhibitory effects on the cisplatin-resistant A2780/Cis ovarian cancer cells

Soon Young Shin [a,†], Hyeryoung Jung [b,†], Seunghyun Ahn [b], Doseok Hwang [b], Hyuk Yoon [b], Jiye Hyun [b], Yeonjoong Yong [b], Hi Jae Cho [b], Dongsoo Koh [c], Young Han Lee [a], Yoongho Lim [b,*]

[a] Department of Biological Sciences, Konkuk University, Seoul 143-701, Republic of Korea
[b] Division of Bioscience and Biotechnology, BMIC, Konkuk University, Hwayang-Dong 1, Kwangjin-Gu, Seoul 143-701, Republic of Korea
[c] Department of Applied Chemistry, Dongduk Women's University, Seoul 136-714, Republic of Korea

ARTICLE INFO

Article history:
Received 28 December 2013
Revised 29 January 2014
Accepted 31 January 2014
Available online 10 February 2014

Keywords:
Chalcone
Cinnamaldehyde
Ovarian cancer
Clonogenicity
QSAR
Aurora A

ABSTRACT

Ovarian carcinoma remains the most lethal among gynecological cancers. Chemoresistance is a clinical problem that severely limits treatment success. To identify potent anticancer agents against the cisplatin-resistant human ovarian cancer cell line A2780/Cis, 26 polyphenols bearing a cinnamaldehyde scaffold were synthesized. Structural differences in their inhibitory effect on clonogenicity of A2780/Cis cells were elucidated using comparative molecular field analysis and comparative molecular similarity indices analysis. Structural conditions required for increased inhibitory activity can be derived based on the analysis of their contour maps. The two most active compounds (**16** and **19**) were selected and further characterized their biological activities. We found that compounds **16** and **19** trigger cell cycle arrest at the G2/M phase and apoptotic cell death in cisplatin-resistant A2780/Cis human ovarian cancer cells. The molecular mechanism of compound **16** was elucidated using in vitro aurora A kinase assay, and the binding mode between the compound **16** and aurora A kinase was interpreted using in silico docking experiments. The findings obtained here may help us develop novel plant-derived polyphenols used for potent chemotherapeutic agents. In conclusion, compounds **16** and **19** could be used as promising lead compounds for the development of novel anticancer therapies in the treatment of cisplatin-resistant ovarian cancers.

1. Introduction

Ovarian cancer is a primary malignancy of women in the Western world, ranking as the fifth leading cause of cancer-related deaths.[1] Ovarian cancer is also the leading cause of death from gynecological cancer. In 2008, it was estimated that there will be 21,650 new ovarian cancer cases in the USA.[2] Early symptoms are frequently very subtle, may include bloating, pelvic pain, difficulty eating, and frequent urination, and are easily confused with other illnesses. Most (more than 90%) of ovarian cancers are classified as epithelial and are believed to arise from the surface (epithelium) of the ovary.[3] Ovarian carcinoma remains the most lethal among gynecological cancers due to the lack of early detection methods and effective treatments for late stage cancers.[4] Due to a lack of effective screening biomarkers, nearly 60–70% of ovarian cancers are diagnosed at advanced stages, with a poor prognosis of about 30% for a 5-year survival rate. Treatment of ovarian cancers involves surgery and chemotherapy, but these are often not effective because of problems with drug resistance and relapse in patients.[5] Although chemotherapy remains a major treatment modality for human ovarian cancer, chemoresistance is a clinical problem that severely limits treatment success because ovarian cancer cells become resistant to drug-induced apoptosis.[6] Cisplatin is a common chemotherapy drug. Platinum-based chemotherapy is the primary treatment for ovarian cancer and is also used to treat other malignancies. However, platinum resistance is multifactorial and complicated.[2] Cisplatin was the first member of a class of platinum-containing anticancer drugs, which now also includes carboplatin and oxaliplatin. These platinum complexes react in vivo, binding to and crosslinking DNA, which ultimately trigger apoptosis. However, the majority of patients with ovarian cancer are not effectively treated by standard cisplatin regimens primarily due to the development of drug resistance.

* Corresponding author. Tel.: +82 2 450 3760; fax: +82 2 3437 6106.
E-mail address: yoongho@konkuk.ac.kr (Y. Lim).
† S.Y. Shin and H. Jung contributed equally to this work.

http://dx.doi.org/10.1016/j.bmc.2014.01.058
0968-0896/

Tangeretin can be used to sensitize cisplatin-resistant human ovarian cancer A2780/Cis.[7] Tangeretin (4′,5,6,7,8-pentamethoxyflavone) belongs to the flavones, which are a family of flavonoids consisting of a C6-C3-C6 skeleton (Fig. 1A). Chalcones showing anticancer effects against prostate, breast, lung, and cervical cancers are one of flavonoids too.[8–11] To find potent anticancer agents against cisplatin-resistant ovarian cancer cells, therefore, methoxychalcones were synthesized in this research. Unlike flavonoids, however, chalcones consist of only two rings connected by an α,β-unsaturated carbonyl group (Fig. 1B). As indicated by bold lines in Figure 1A and B, flavone and chalcone contain a cinnamaldehyde skeleton. While chalcone is composed of two separate rings, flavonoids have two attached rings. Similar to flavonoids, 2*H*-chromen consists of two attached rings (Fig. 1C). To obtain compounds with two attached rings, four methoxy-2*H*-chromene-3-carbaldehydes derived from 2*H*-chromen were synthesized, which also have a cinnamaldehyde scaffold (Fig. 1D). Few studies have evaluated the anticancer effects of chalcones against ovarian cancer.[12] Here, the anticancer effects of chalcones and 2*H*-chromene-3-carbaldehydes bearing a cinnamaldehyde scaffold against ovarian cancer were evaluated using comparative molecular field analysis and comparative molecular similarity indices analysis. The 26 compounds tested here contain a common feature, such as cinnamaldehyde, and overall have similar structures. Because differences in their anticancer effects may not be distinguished at the cellular level, we adopted a clonogenic assay against the cisplatin-resistant ovarian cancer cell line, A2780/Cis. The anticancer effects of chalcones and 2*H*-chromene-3-carbaldehydes against the A2780/Cis cisplatin-resistant ovarian cancer cell lines have not been reported. Because the compounds tested here contain a cinnamaldehyde scaffold, they all can be classified as plant-derived polyphenols. To identify structural changes in polyphenols that increases their effects on the clonogenicity of A2780/Cis human ovarian cancer cells, the relationships between 26 polyphenols and their activities were elucidated. In addition, for polyphenols showing good inhibitory effects on cancer cells further biological experiments including flow cytometry, Western blot analysis, and immunofluorescent microscopy were carried out. The molecular mechanism of the compound showing good cell growth inhibitory effect was elucidated using in vitro aurora A kinase assay, and the binding mode between the compound and aurora A kinase was interpreted using in silico docking experiments. The findings obtained here may help us develop novel plant-derived polyphenols used for potent chemotherapeutic agents.

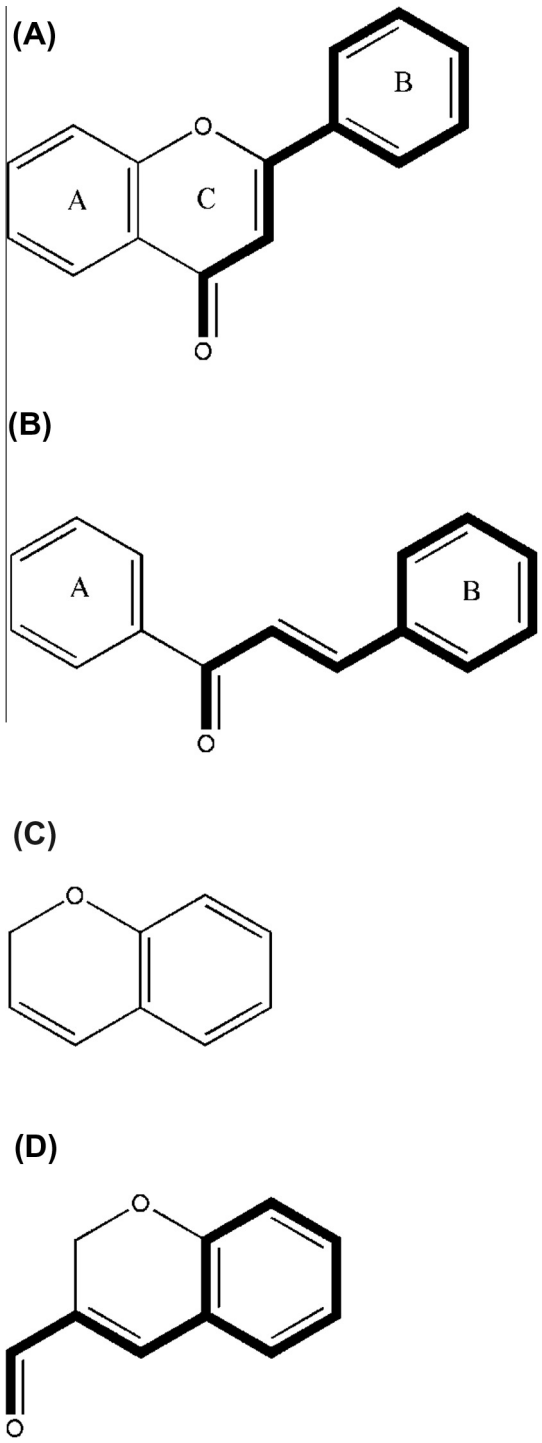

Figure 1. Design of polyphenols bearing a cinnamaldehyde scaffold. Structures of (A) flavone, (B) chalcone, (C) 2*H*-chromene, and (D) 2*H*-chromene-3-carbaldehyde. Bold lines denote the cinnamaldehyde scaffold.

2. Results and discussion

2.1. Relationships between polyphenols bearing a cinnamaldehyde scaffold and their anticancer activities

Initially, the 26 compounds listed in Table 1 were synthesized. The three dimensional (3D) structures of the compounds must be identified to determine relationships between physical and chemical properties of the compounds and their biological activities. All calculations in this experiment were performed on an Intel Core 2 Quad Q6600 (2.4 GHz) Linux PC with the molecular modeling package Sybyl 7.3 (Tripos, St. Louis, MO).[13] To distinguish small biological differences caused by compounds with similar structures, a clonogenic survival assay was used because it measures the long-term cytotoxicity of anticancer agents.[14] The inhibitory effects of 26 polyphenols from the clonogenic assay on A2780/Cis human ovarian cancer cells (Health Protection Culture Collections, Salisbury, UK) at four different concentrations (0, 5, 10, and 20 μM) are shown in Figure 2 and their half-maximal cell growth inhibitory concentration, (GI_{50}) values are listed in Table 1. Compound **16** was showing the best inhibitory effect and its GI_{50} value was 3.87 μM. Comparative molecular field analysis (CoMFA) and comparative molecular similarity indices analysis (CoMSIA) were used for the quantitative structure–activity relationship (QSAR) calculations. The 26 compounds listed in Table 1 were randomly divided into a training set of 21 compounds and a test set of 5 compounds (**7**, **8**, **13**, **21**, and **22**). The former was used to create QSAR models, and the later was used to validate the models. The test set was analyzed by hierarchical clustering.[15] As shown in Figure S1 in Supplementary data contents, most compounds chosen for the test

Table 1
Structures and nomenclature of the 26 compounds and their biological activities (the half-maximal cell growth inhibitory concentration, GI_{50}) obtained from the clonogenic survival density of A2780/Cis ovarian cancer cells and their negative logarithmic scale of GI_{50} (pGI_{50})

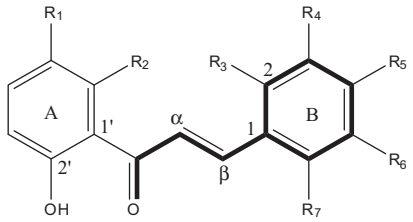

Compound	R_1	R_2	R_3	R_4	R_5	R_6	R_7	GI_{50}/μM	pGI_{50}
1	H	H	OCH_3	H	H	H	H	11.69	1.93
2	H	H	H	H	OCH_3	H	H	15.94	1.80
3	H	H	H	OCH_3	H	OCH_3	H	13.69	1.86
4	H	H	OCH_3	OCH_3	H	H	H	14.38	1.84
5	H	H	OCH_3	H	OCH_3	H	H	14.96	1.83
6	H	H	H	H	H	H	H	13.45	1.87
7*	H	H	OCH_3	OCH_3	OCH_3	H	H	14.30	1.84
8*	H	OCH_3	H	OCH_3	H	OCH_3	H	11.44	1.94
9	H	OCH_3	OCH_3	H	H	H	H	9.55	2.02
10	H	OCH_3	H	OCH_3	H	H	H	9.64	2.02
11	H	OCH_3	H	H	OCH_3	H	H	15.38	1.81
12	H	OCH_3	OCH_3	OCH_3	H	H	H	9.67	2.01
13*	H	OCH_3	OCH_3	H	OCH_3	H	H	9.55	2.02
14	H	OCH_3	OCH_3	OCH_3	OCH_3	H	H	18.38	1.74
15	H	OCH_3	OCH_3	H	OCH_3	OCH_3	H	19.21	1.72
16	H	OCH_3	OCH_3	H	OCH_3	H	OCH_3	3.87	2.41
17	OCH_3	H	H	OCH_3	H	OCH_3	H	11.30	1.95
18	OCH_3	H	OCH_3	H	OCH_3	OCH_3	H	>20	1.70
19	OCH_3	H	OCH_3	H	OCH_3	H	OCH_3	3.95	2.40
20	OCH_3	H	H	OCH_3	H	H	H	10.13	1.99
21*	OCH_3	H	OCH_3	OCH_3	H	H	H	16.96	1.77
22*	OCH_3	H	OCH_3	H	OCH_3	H	H	19.77	1.70

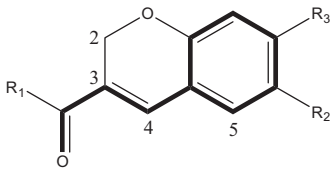

Compound	R_1	R_2	R_3	GI_{50}/μM	pGI_{50}
23	H	H	OCH_3	>20	1.70
24	H	OCH_3	H	>20	1.70
25	CH_3	OCH_3	H	>20	1.70
26	CH_3	H	OCH_3	>20	1.70

The asterisk (*) denotes a test set used for calculations of the quantitative structure–activity relationships. Bold lines indicate a cinnamaldehyde scaffold.

set belong to separate structural groups. Therefore, the test set can be used to validate whether the QSAR models in this experiment are reliable. To identify interactions between probe atoms and the rest of the molecule, the training set was aligned using the Sybyl/DATABASE Alignment module. Because compounds in the data set are not homogeneous, heavy atoms contained in the cinnamaldehyde skeleton were used for alignment where a consistent superposition was observed (Fig. S2 in Supplementary data contents).

To elucidate relationships between the molecular structures of a training set and their clonogenicities against A2780/Cis ovarian cancer cells, CoMFA was performed, which creates electrostatic and steric fields. To investigate the linear correlation between the calculated fields and the biological activities, partial least squares regression was adopted. Twelve CoMFA models were built using the region focusing method to enhance the cross-validation correlation coefficient (q^2) and non-cross-validated coefficient (r^2) values and to refine the model. Here, standard deviation coefficient values ranged from 0.3 to 1.2 and grid spacing values from 0.5 to 1.5. To select the best model, a validation process was required. The cross-validation analysis was performed using the leave-one-out method. The cross-validated correlation coefficient (q^2) and non-cross-validated correlation coefficient (r^2) were calculated based on the overall compounds in the training set. Among the models generated from CoMFA, the model showing the best cross-validated correlation coefficient ($q^2 = 0.933$) was chosen for the further analysis. Partial least square (PLS) analysis was carried out to establish a linear relationship between the biological activity and the resulting field matrix of 26 compounds. The cross-validated analysis was performed using the leave-one-out (LOO) method. The final non-cross-validated ($r^2 = 0.992$) analysis was performed using the optimal number of components ($N = 6$) obtained from the LOO method. In the PLS analysis, the standard error of estimate and F value were determined to be 0.022, and 280.884, respectively. The best CoMFA model was obtained by the region focusing method. To evaluate the CoMFA model, the activities of the compounds contained in the training set were predicted and compared to the experimental data as listed in Table 2. The residuals between the experimental and predicted values for the training set ranged from 0% to 2.35%. To validate the QSAR model, five compounds (**7**, **8**, **13**, **21**, and **22**) were selected as a test set. Their residuals ranged between 1.55% and 13.53%. Thus, the

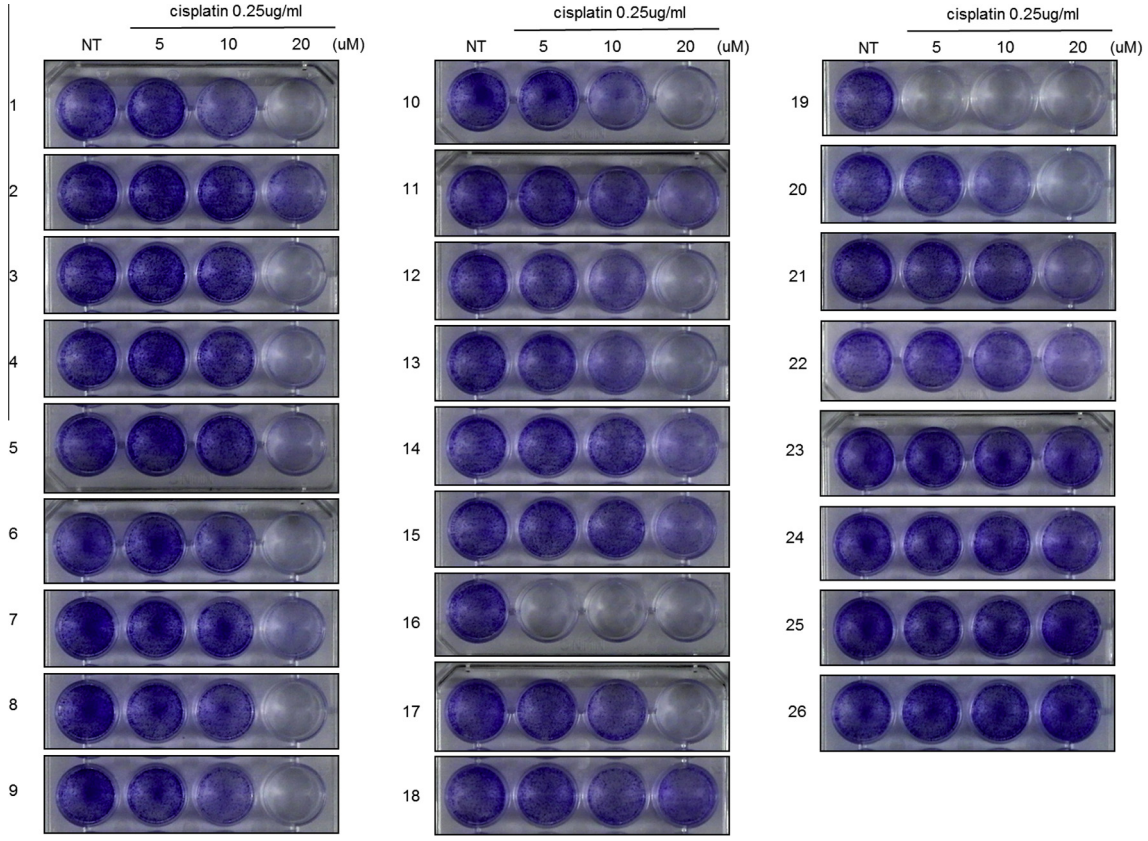

Figure 2. Effects of synthetic compounds with the cinnamaldehyde scaffold on the clonogenicity of A2780/Cis human ovarian cancer cells. A2780/Cis cells (5×10^3 cells/well) were plated and cultured for 7 days in the absence or presence of different concentrations of the test compounds. Similar results were obtained from two other independent experiments.

Table 2
The residual values between experimental and predicted values for the training set and test set

	Experimental data/pGI_{50}	CoMFA		CoMSIA	
		Predicted value/pGI_{50}	Residual[a] (%)	Predicted value/pGI_{50}	Residual[a] (%)
1	1.93	1.91	0.02	1.91	0.02
2	1.80	1.79	0.01	1.81	−0.01
3	1.86	1.85	0.01	1.84	0.02
4	1.84	1.84	0.00	1.88	−0.04
5	1.83	1.84	−0.01	1.76	0.07
6	1.87	1.89	−0.02	1.95	−0.08
7*	1.84	1.70	0.14	1.74	0.10
8*	1.94	1.91	0.03	1.89	0.05
9	2.02	2.00	0.02	1.97	0.05
10	2.02	2.01	0.01	1.97	0.05
11	1.81	1.83	−0.02	1.83	−0.02
12	2.01	1.98	0.03	1.96	0.05
13*	2.02	1.9	0.12	1.83	0.19
14	1.74	1.74	0.00	1.79	−0.05
15	1.72	1.73	−0.01	1.76	−0.04
16	2.41	2.42	−0.01	2.42	−0.01
17	1.95	1.96	−0.01	1.92	0.03
18	1.70	1.72	−0.02	1.75	−0.05
19	2.40	2.39	0.01	2.41	−0.01
20	1.99	2.01	−0.02	1.99	0.00
21*	1.77	1.95	−0.18	1.95	−0.18
22*	1.70	1.93	−0.23	1.82	−0.12
23	1.70	1.70	0.00	1.66	0.04
24	1.70	1.68	0.02	1.73	−0.03
25	1.70	1.74	−0.04	1.75	−0.05
26	1.70	1.67	0.03	1.65	0.05

Asterisk(*) denotes the test set.
[a] [(experimental data)−(values predicted by CoMFA or CoMSIA)] × 100.

CoMFA model obtained here is reliable. The plot of the experimental data versus the values predicted is shown in Figure S3 in Supplementary data contents.

While CoMFA provides information on only the steric and electrostatic effects, CoMSIA gives information on the steric and electrostatic effects as well as the hydrophobic, hydrogen bond (H-bond) donor and acceptor effects. Among several CoMSIA models, the best model displaying the best cross-validated value ($q^2 = 0.793$) was selected. The correlation coefficient (r^2) was 0.954. In the PLS statistical parameters, the number of components, the standard error of estimate, and the *F* values were 6, 0.053 and 48.480, respectively. Like CoMFA, to evaluate the CoMSIA model, the activities for the training and test sets were predicted and compared to the experimental data. A comparison of the experimental data and the values predicted by CoMSIA is listed in Table 2, and the plot of the experimental data versus the values predicted is shown in Figure S4 in Supplementary data contents. In the training set, their residuals between the experimental and predicted values ranged from 0% to 4.28% and in the case of test set, their residuals ranged from 2.58% to 10.17%. Therefore, the CoMSIA model is reliable.

In order to visualize the relationships between the structures of 26 compounds and their inhibitory activities on clonogenicity, CoMFA contour maps were generated using the Sybyl 7.3 program. The steric and electrostatic field descriptors contributed 50.3% and 49.7%, respectively. In the case of the steric field, the steric bulky favored region contributed 75% and the disfavored region contributed 25%. Compound **16** showed the best inhibitory effect and is embedded in the contour map (Fig. 3). Likewise, the contour map for the electrostatic field was generated, where the electropositive group favored region and the electronegative group favored region contributed 70% and 30%, respectively. Changes in the methoxy groups are the only differences between the compounds in this study, so the electrostatic field gives little information to distinguish between favored and disfavored contours. As shown in Figure 3, green and yellow contours near the chalcone B-ring indicate that the absence of a bulky group at C-5 and the presence of bulky group at C-6 are required for the inhibitory activity. This is based on comparisons of compounds **18**, **19**, and **22** and of compounds **13**, **15**, and **16**. In addition, the bulky group at C-3 position decreased inhibition. This is demonstrated based on observations with compounds **13** and **14**. Like the bulky group at C-3, that at C-4 decreased inhibition: compounds **5** and **14** showed worse activities than compounds **1** and **12**, respectively. The green contour near the chalcone A-ring indicates that the A-ring is required for high inhibitory activity. The four 2*H*-chromene-3-carbaldehyde derivatives lacking A-rings have GI_{50} values above 20 μM.

With a same method of CoMFA, CoMSIA countour maps were generated. CoMSIA provides information about the steric and electrostatic field as well as hydrophobic, H-bond donor, and acceptor fields. In this experiment, CoMSIA model selected only the steric, electrostatic, hydrophobic, and H-bond acceptor field

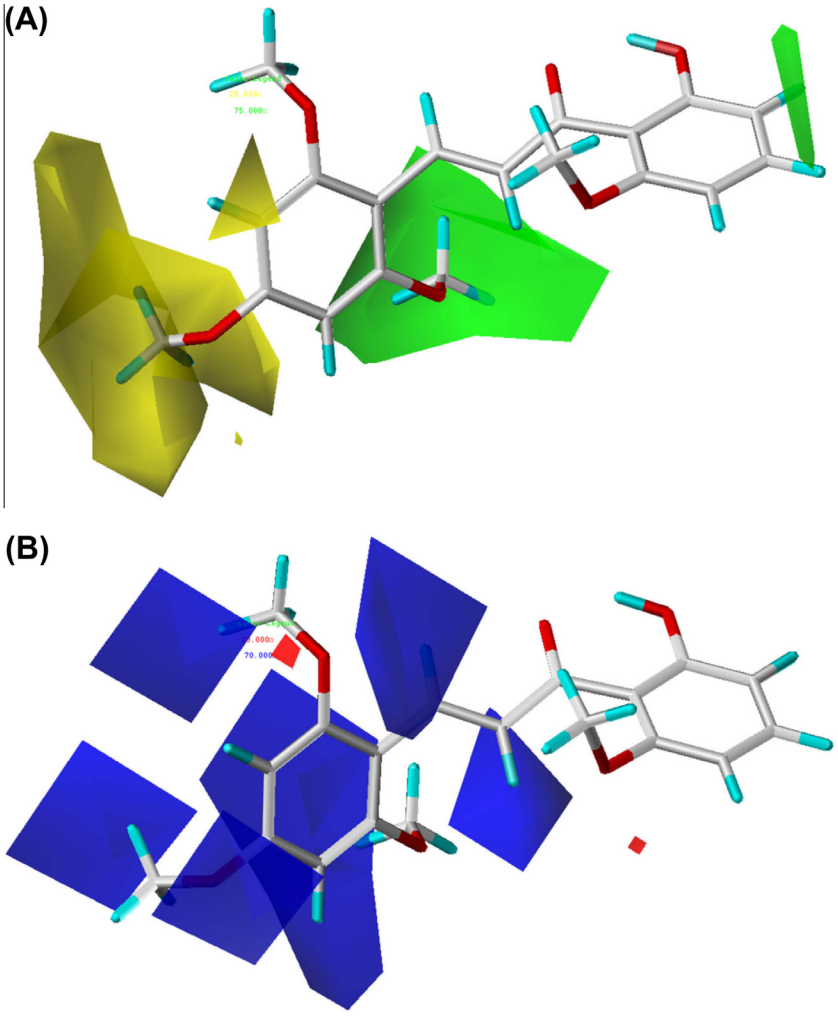

Figure 3. CoMFA contour maps. (A) The steric field contours are shown in green (more bulkiness favored) and yellow (less bulkiness favored). (B) The electrostatic field contours are shown in red (electronegative substituents favored) and blue (electropositive substituents favored).

descriptors contributed at 15%, 49.7%, 31%, and 4.3%, respectively. More bulkiness favored, less bulkiness favored, electronegative favored, electropositive favored, hydrophobic favored, hydrophobic disfavored, H-bond acceptor favored, and H-bond acceptor disfavored contours are shown in the CoMSIA contour maps (Fig. 4). In the case of the steric field, the steric bulky favored region contributed 79% and the disfavored region contributed 21%, and in the electrostatic field, the electropositive favored region contributed 77% and the electronegative favored region contributed 23%. In the case of the hydrophobic field, the hydrophobic favored region contributed 71% and the disfavored region contributed 29%, and in the case of the H-bond acceptor field, the H-bond acceptor favored region contributed 35% and the disfavored region contributed 65%. Because information about the steric and electrostatic fields from CoMSIA maps is similar to that from CoMFA, the contour maps regarding the hydrophobic and H-bond acceptor fields were analyzed. As shown in Fig. 4, an orange contour near C-4 position indicates that hydrophobic substituents at the position are increased for the activity. For examples, compounds **1**, **6**, and **12** show better activity than compounds **5**, **2**, and **14**, respectively. In contrast, a hydrophilic group at C-6 position increased inhibition. Compounds **16** and **19**, which bear an $-OCH_3$ at C-6, showed better inhibition than compounds **13** and **22**, respectively. The orange contour near the chalcone A-ring shows that the presence of hydrophobic aromatic ring is required for inhibitory activity. In case of the H-bond acceptor field, a cyan contour is observed at 2′-OH. This field distinguishes between twenty-two hydroxychalcones and four 2*H*-chromene-3-carbaldehydes. So, the 2′-hydroxy group is required for the inhibitory effect.

Based on the analysis of CoMFA and CoMSIA contour maps, the structural conditions to show better inhibitory effects on the clonogenicity of A2780/Cis ovarian cancer cells can be summarized as shown in Figure 5. 2′-Hydroxy group of chalcones A-ring favors H-bond donor group. And, the existence of hydrophobic and bulky chalcone A-ring increases the inhibitory activity. Carbonyl group favors hydrophilic and H-bond acceptor. The less bulkiness substituents at C-3 and C-5, less bulkiness or hydrophobic substituents at C-4, more bulkiness or hydrophilic substituents at C-6 position increase the inhibitory effects.

2.2. Evaluation of biological activities of selective polyphenols

To test the effects of compounds **16** and **19** on the inhibition of cell growth, cisplatin-resistant A2780/Cis human ovarian cancer cells were exposed to varying concentrations of compounds **16** and **19** (1–20 μM) for 24 or 48 h, and the cell proliferation rate was measured using a Cell Counting Kit-8. Proliferation of A2780/Cis cells was significantly inhibited by treatment with both compounds **16** and **19** in a dose- and time-dependent manner as shown in Figure 6A.

We next investigated whether compounds **16** and **19** inhibit cell proliferation due to blockade of the cell cycle progression. Flow cytometry analysis revealed that treatment of A2780/Cis cells with compounds **16** and **19** at 20 μM for 24 h strongly increased a population of cells in G2/M phase of the cell cycle (control, 29.4%; **16**, 70.99%; **19**, 68.27%), with a concomitant decrease in the number of cells in G1 (control, 45.33%; **16**, 3.36%; **19**, 3.53%) and the S phase (control, 17.24%; **16**, 4.33%; **19**, 4.09%) as shown in Figure 6B. Notably, the population of sub-G1 cells, a typical marker of apoptosis, was increased (control, 7.76%; **16**, 17.06%; **19**, 16.54%) by treatment with both compounds **16** and **19**. These data clearly demonstrate that both compounds **16** and **19** inhibit growth of A2780/Cis cells through induction of cell cycle arrest at the G2/M phase and apoptosis.

The caspases play a critical role in the progression of apoptosis induced by diverse chemotherapeutic agents. To determine whether caspases are involved in compound **16**- and **19**-induced apoptosis, Western blot analysis was performed using antibodies recognizing the cleaved active forms of caspase-7. Treatment of A2780/Cis cells with 20 μM compound **16** or **19** stimulated the cleavage of caspase-7 after 24 h of treatment (Fig. 6C). The processing of native 113-kDa poly(ADP-ribose) polymerase (PARP) to the

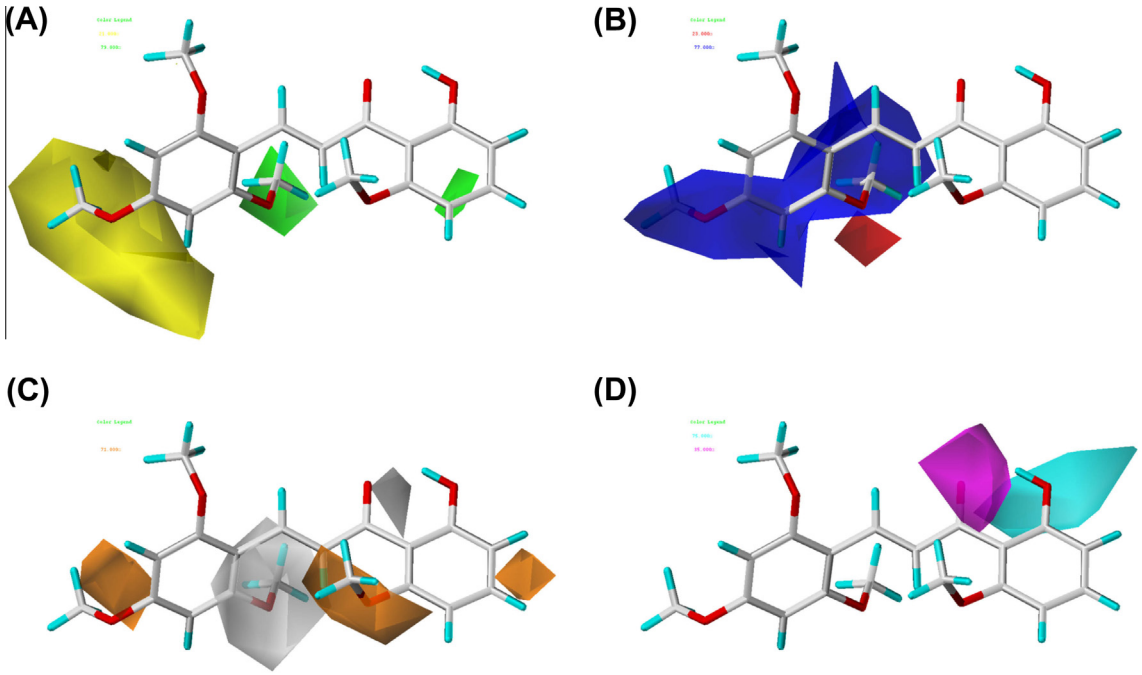

Figure 4. CoMSIA contour maps. (A) The steric field contours are shown in green (more bulkiness favored) and yellow (less bulkiness favored). (B) The electrostatic field contours are shown in red (electronegative substituents favored) and blue (electropositive substituents favored). (C) Hydrophobic field contours are shown in orange (hydrophobic favored) and white (hydrophobic disfavored). (D) H-bond acceptor filed contours are shown in magenta (H-bond acceptor favored) and cyan (H-bond acceptor disfavored).

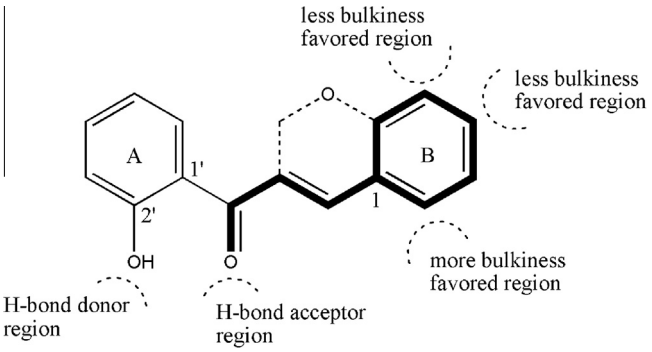

Figure 5. Structural conditions to show better inhibitory effects on the clonogenicity of A2780/Cis ovarian cancer cells. From the analysis of CoMFA and CoMSIA results, H-bond donor group at 2′-hydroxy position, the existence of hydrophobic and bulky chalcone A-ring, the less bulkiness substituents at C-3 and C-5, less bulkiness or hydrophobic substituents at C-4, and more bukiness or hydrophilic substituents at C-6 position are required for the inhibitory activity. Bold lines indicate a cinnamaldehyde scaffold.

89-kDa and 24-kDa is the result of caspase-3- or caspase-7-catalyzed cleavage.[16] The amount of this typical cleaved form of PARP was also increased after 24 h of treatment. The presence of compound **19**-induced cleaved active caspase-7 was confirmed by immunofluorescent microscopy (Fig. 6D). We also observed that compound **19**-exposed cells were characterized by shrunken and fragmented nuclei with condensed chromatin, indicative of apoptosis induction.

2.3. In vitro inhibitory effect of compound 16 on aurora A kinase and their molecular binding mode

Compound **16** inhibits growth of A2780/Cis cells through induction of cell cycle arrest at the G2/M phase. Aurora A kinase is known to be involved in cell cycle arrest at the G2/M phase. Therefore, in vitro aurora A (aurA) kinase assay was performed for compound **16**. AurA belongs to serine/threonine kinases and is one of aurora family A, B, and C.[17] Since aurA is overexpressed in various tumors including ovary, colon, breast and skin cancers, and its overexpression is caused by failed cytokinesis, it is a target for chemotherapeutic agents.[18] In vitro aurA kinase assay of compound **16** showed the half-maximal inhibitory concentration (IC_{50}) of 66.4 μM. Because aurA may not be a real molecular target of compound **16**, worse GI_{50} value of compound **16** than the IC_{50} value can be explained.

To elucidate the binding mode between compound **16** and aurA, in silico docking experiments were performed. The three dimensional (3D) structure of compound **16** was determined in our lab

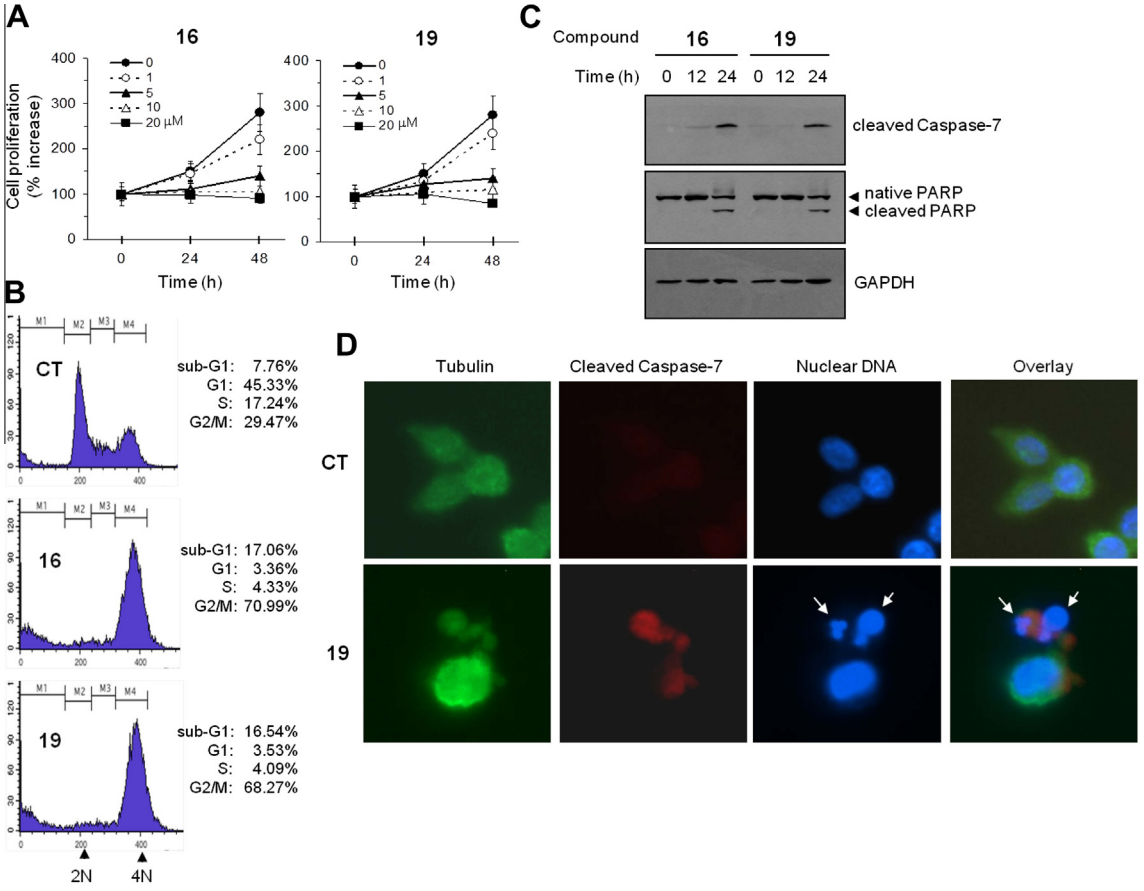

Figure 6. Evaluation of antitumor activities of compounds **16** and **19**. (A) Effects of compounds **16** and **19** on the inhibition of cisplatin-resistant human ovarian cancer cells. A2780/Cis cells were seeded onto 96-well culture plates and treated with various concentrations of **16** and **19** for the indicated lengths of time. Cellular proliferation was measured using Cell Counting Kit-8. The data shown represent the mean ± SD for one experiment performed in triplicate. (B) Effects of compounds **16** and **19** on the cell cycle and apoptosis. A2780/Cis cells were treated with vehicle (DMSO) or 20 μM compounds **16** and **19**. After 24 h, the cells were harvested, fixed with ethanol, and stained with propidium iodide. The DNA content was analyzed using flow cytometry. The percentages of the cell population at each phase of the cell cycle are indicated in each histogram. *x*-axis, cell counts; *y*-axis, DNA contents; CT, DMSO-treated control group; M1, sub-G1; M2, G1; M3, S; M4, G2/M; 2N, diplod; 4N, tetraploid. (C) Effects of compounds **16** and **19** on caspase-7 activation. A2780/Cis cells were treated with 20 μM compound **16** or **19** for 12 or 24 h, and whole cell lysates were analyzed for the cleaved forms of caspase-7 and PARP by Western blotting. GAPDH was used as an internal control. (D) Effects of compound **19** on the cleavage of caspase-7 and DNA fragmentation. A2780/Cis cells were treated with 20 μM compound **19** for 24 h. Microtubules or cleaved caspase-7 were stained by incubation with anti-α-tubulin or anti-cleaved caspase-7 (Asp198) antibody for 90 min and then with Alexa-Fluor 488-conjugated (green signal) and Alexa-Fluor 555-conjugated (red signal) secondary antibodies for 30 min. Chromosomal DNA (blue) was stained with TO-PRO-3 iodide. Arrows indicate fragmented and condensed nuclei of apoptotic cells.

using X-ray crystallography and that of aurA was adapted from the X-ray crystallographic structure deposited in the protein data bank (PDB) as 3o50.pdb.[19] This 3D protein structure consists of a homodimer, but the chain B was selected because it contains more residues than the chain A. Its apo-protein was prepared using the Sybyl7.3 program (Tripos, St. Louis, MO) and named 3o50B.pdb. First, to confirm whether our docking procedure works well, the ligand contained in 3o50B.pdb, LJE (*N*-{3-methyl-4-[(3-pyrimidin-4-ylpyridin-2-yl)oxy]phenyl}-3-(trifluoromethyl)benzamide) was docked into 3o50B.pdb. The residues participating in the binding site were analyzed using the LigPlot program.[20] These residues were compared with the residues determined by the LigPlot analysis of the crystallographic structure (3o50.pdb) deposited in the PDB. Thirteen residues including Gly140, Lys141, Val147, Lys162, Glu181, Leu210, Glu211, Tyr212, Ala213, Asn261, Leu263, Ala273, and Phe275 are identical to each other. Therefore, the apo-protein 3o50B.pdb was used for *in silico* docking experiments of compound **16** and aurA. Thirty compound **16**–aurA complexes were obtained by 30 iteration docking process and their binding energy ranged between −26.29 and −19.49 kcal/mol. Of 30 complexes, a complex showing the best docking pose was selected because the binding energy was low enough to form the ligand–protein complex. This complex was analyzed using LigPlot. As shown in Figure 7A, 11 residues including Lys141, Gly142, Lys143, Val147, Lys162, Leu210, Lys258, Glu260, Asn261, Ala273, and Phe275 were observed in the binding site and seven residues such as Lys141, Val147, Lys162, Leu210, Asn261, Ala273, and Phe275 were found in both the binding site of the crystallographic

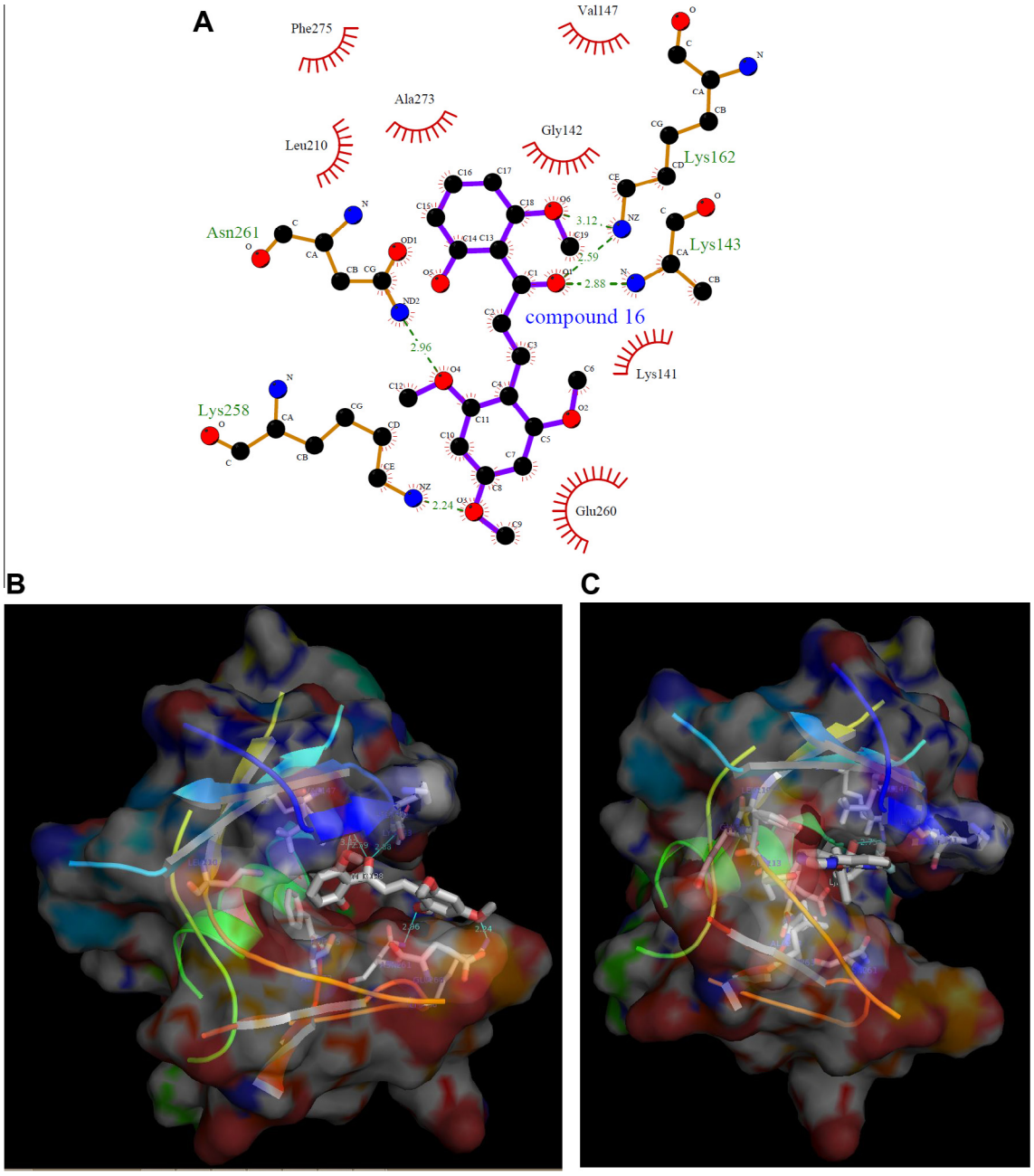

Figure 7. (A) The residues surrounding the ligand, (*N*-{3-methyl-4-[(3-pyrimidin-4-ylpyridin-2-yl)oxy]phenyl}-3-(trifluoromethyl)benzamide, LJE), embedded in the chain B of aurora A kinase (3o50B.pdb) analyzed using the LigPlot program. Eleven residues including Lys141, Gly142, Lys143, Val147, Lys162, Leu210, Lys258, Glu260, Asn261, Ala273, and Phe275 were observed in the binding site. (B) The 3D image of the binding site of the compound **16**—aurora A complex generated by the PyMOL program. (C) The 3D image of the binding site of the LJE-aurora A complex generated by the PyMOL program.

structure (3o50.pdb) deposited in the PDB and the compound **16**–aurA complex. In addition to seven residues, the remained five residues lie to the surroundings of seven residues. While 11 residues of the binding site of 3o50B.pdb show the hydrophobic interactions and a residue, Lys162, forms hydrogen bonds (H-bonds) with the ligand, LJE, seven residues of the compound **16**–aurA complex participate in the hydrophobic interactions and four residues including Lys143, Lys162, Lys258, and Asn261 form H-bonds. The 3D image of the binding site of the compound **16**–aurA complex was generated by the PyMOL program (Fig. 7B). While the ligand of 3o50B.pdb resides inside the binding pocket as shown in Figure 7C, compound **16** is located in the entrance of the binding site as shown in Figure 7B. Even the number of the residues participating in the binding site of 3o50B.pdb with its ligand, 11, is same as that of the compound **16**–aurA complex, the binding condition of the ligand of 3o50B.pdb is different with that of the compound **16**–aurA complex. This may cause the result where the IC_{50} value (66.4 μM) obtained from in vitro aurA kinase assay of compound **16** is worse than the GI_{50} value (3.87 μM) obtained from the clonogenic survival density of A2780/Cis ovarian cancer cells.

3. Conclusion

The structural conditions required for high inhibitory activities on cell growth could be summarized based on the analysis of CoMFA and CoMSIA. Our results suggest that the absence of a bulky group near C-3′, C-5′, and C-5, the presence of a bulky group near C-6′, the existence of an A-ring in the test compounds, and the existence of an H-bond acceptor group near the C-2 position are required for potent antitumor activity. We selected the two most active compounds (**16** and **19**) to further characterize their biological activities. Cell proliferation measurement, flow cytometry analysis, and Western blot analysis demonstrated that both **16** and **19** compounds induce cell cycle arrest at the G2/M phase and apoptotic cell death in cisplatin-resistant A2780/Cis human ovarian cancer cells. In conclusion, compounds **16** and **19** could be used as a promising lead compounds for the development of novel anticancer therapies in the treatment of cisplatin-resistant ovarian cancers.

4. Experimental protocols

4.1. Chemistry

Melting points were measured using Mel-Temp II (LabX, Midland, ON, Canada) and were uncorrected. Ultraviolet/visible (UV/VIS) spectra and infrared (IR) spectra were collected on a 50Conc UV-Visible spectrophotometer (Varian) and FT-IR 4200 (JASCO, Easton, MD) with ATR (Attenuated Total Reflection, ATR PR0450-S), respectively. Column chromatography purifications were performed on Silica gel 60 (70–230 mesh, Merck, Whitehouse Station, NJ). All NMR experiments were performed on a Bruker Avance 400 spectrometer system (9.4 T; Bruker, Karlsruhe, Germany) at 298 K. The synthetic compounds were dissolved in DMSO-d_6. The ^1H and ^{13}C chemical shifts of the deuterated solvent were referenced to tetramethylsilane (TMS). The NMR samples were prepared at approximately 50 mM and were transferred to a 2.5-mm NMR tube. For the one-dimensional ^1H and ^{13}C NMR experiments, the relaxation delays were 1 and 3 s, respectively, and the 90° pulses were 11.8 and 15.0 μs, respectively. The ^1H and ^{13}C spectral widths were 4800 and 21,000 Hz, respectively. For the two-dimensional experiments, including correlated spectroscopy (COSY), total correlated spectroscopy (TOCSY), nuclear Overhauser enhancement spectroscopy (NOESY), heteronuclear multiple quantum coherence (HMQC), and heteronuclear multiple bonded connectivities (HMBC), all data were acquired with 2K × 256 data points ($t_2 \times t_1$). The mixing time for the NOESY experiment was 1 s, and the long-range delay for HMBC was 70 ms. Zero-filling of 2 K and the sine-squared bell window function were applied prior to Fourier transformation using XWin-NMR (Bruker).[21] All NMR data were analyzed using Sparky.[22] All mass spectra were collected on a high-resolution electron impact ionization mass spectrometer (HREIMS, JMS700, Jeol Ltd., Tokyo, Japan) with the help of the Korea Basic Science Institute at Daegu, Korea.[21]

4.2. Preparation of chalcone derivatives 1–22

The synthetic procedure of the 2′-hydroxychalcone derivatives (**1**–**22**) and their NMR and HREIMS data were reported previously.[21] The physicochemical properties including color, melting point, yield, purity, UV/vis, and IR data for 2′-hydroxychalcones (**1**–**22**) are as follows:

4.2.1. (*E*)-1-(2-Hydroxyphenyl)-3-(2-methoxyphenyl)prop-2-en-1-one (1)

Color: yellow; mp 110–112 °C (literature data 111–112 °C);[23] Yield: 66%; purity: 90%; UV/vis λ_{max} (in acetonitrile): 365 nm; IR (cm^{-1}): 1638 (C=O), 1462 (C=C).

4.2.2. (*E*)-1-(2-Hydroxyphenyl)-3-(4-methoxyphenyl)prop-2-en-1-one (2)

Color: yellow; mp 91–92 °C (literature data 92 °C);[24] Yield: 64%; purity: 99%; UV/vis λ_{max} (in acetonitrile): 365 nm; IR (cm^{-1}): 1635 (C=O), 1441 (C=C).

4.2.3. (*E*)-3-(3,5-Dimethoxyphenyl)-1-(2-hydroxyphenyl)prop-2-en-1-one (3)

Color: orange; mp 109–110 °C (literature data 110–111 °C);[25] Yield: 26%; purity: 98%; UV/vis λ_{max} (in acetonitrile): 385 nm; IR (cm^{-1}): 1638 (C=O), 1441 (C=C).

4.2.4. (*E*)-3-(2,3-dimethoxyphenyl)-1-(2-hydroxyphenyl)prop-2-en-1-one (4)

Color: yellow; mp 92–93 °C; Yield: 88%; purity: 95%; UV/vis λ_{max} (in acetonitrile): 360 nm; IR (cm^{-1}): 1636 (C=O), 1478 (C=C).

4.2.5. (*E*)-1-(2-Hydroxyphenyl)-3-(2,4,6-trimethoxyphenyl)prop-2-en-1-one (5)

Color: yellow; mp 102–103 °C; Yield: 72%; purity: 99%; UV/vis λ_{max} (in acetonitrile): 385 nm; IR (cm^{-1}): 1672 (C=O), 1471 (C=C).

4.2.6. (*E*)-1-(2-Hydroxyphenyl)-3-phenylprop-2-en-1-one (6)

Color: yellow; mp 87–88 °C (literature data 88–89 °C);[26] Yield: 58%; purity: 99%; UV/vis λ_{max} (in acetonitrile): 325 nm; IR (cm^{-1}): 1638 (C=O), 1483 (C=C).

4.2.7. (*E*)-1-(2-Hydroxyphenyl)-3-(2,4,5-trimethoxyphenyl)prop-2-en-1-one (7)

Color: yellow; mp 130–131 °C (literature data 131–132 °C);[27] Yield: 62%; purity: 99%; UV/vis λ_{max} (in acetonitrile): 370 nm; IR (cm^{-1}): 1627 (C=O), 1460 (C=C).

4.2.8. (*E*)-3-(3,5-Dimethoxyphenyl)-1-(2-hydroxy-6-methoxyphenyl)prop-2-en-1-one (8)

Color: dark yellow; mp 109–110 °C; Yield: 52%; purity: 96%; UV/vis λ_{max} (in acetonitrile): 350 nm; IR (cm^{-1}): 1631 (C=O), 1448 (C=C).

4.2.9. (*E*)-1-(2-Hydroxy-6-methoxyphenyl)-3-(2-methoxyphenyl)prop-2-en-1-one (9)

Color: orange; mp 101–102 °C; Yield: 63%; purity: 99%; UV/vis λ_{max} (in acetonitrile): 355 nm; IR (cm^{-1}): 1617 (C=O), 1455 (C=C).

4.2.10. (*E*)-1-(2-Hydroxy-6-methoxyphenyl)-3-(3-methoxyphenyl)prop-2-en-1-one (10)

Color: yellow; mp 85–86 °C; Yield: 85%; purity: 93%; UV/vis λ_{max} (in acetonitrile): 355 nm; IR (cm^{-1}): 1629 (C=O), 1452 (C=C).

4.2.11. (*E*)-1-(2-Hydroxy-6-methoxyphenyl)-3-(4-methoxyphenyl)prop-2-en-1-one (11)

Color: orange; mp 115–116 °C (literature data 113–115 °C);[28] Yield: 81%; purity: 91%; UV/vis λ_{max} (in acetonitrile): 355 nm; IR (cm^{-1}): 1622 (C=O), 1453 (C=C).

4.2.12. (*E*)-3-(2,3-Dimethoxyphenyl)-1-(2-hydroxy-6-methoxyphenyl)prop-2-en-1-one (12)

Color: yellow; mp115–116 °C; Yield: 89%; purity: 99%; UV/vis λ_{max} (in acetonitrile): 355 nm; IR (cm^{-1}): 1629 (C=O), 1452 (C=C).

4.2.13. (*E*)-3-(2,4-Dimethoxyphenyl)-1-(2-hydroxy-6-methoxyphenyl)prop-2-en-1-one (13)

Color: yellow; mp 113–114 °C (literature data 106–108 °C);[29] Yield: 96%; purity: 85%; UV/vis λ_{max} (in acetonitrile): 375 nm; IR (cm^{-1}): 1623 (C=O), 1451 (C=C).

4.2.14. (*E*)-1-(2-Hydroxy-6-methoxyphenyl)-3-(2,3,4-trimethoxyphenyl)prop-2-en-1-one (14)

Color: yellow; mp119–120 °C; Yield: 93%; purity: 99%; UV/vis λ_{max} (in acetonitrile): 365 nm; IR (cm^{-1}): 1625 (C=O), 1455 (C=C).

4.2.15. (*E*)-1-(2-Hydroxy-6-methoxyphenyl)-3-(2,4,5-trimethoxyphenyl)prop-2-en-1-one (15)

Color: orange; mp 132–133 °C; Yield: 58%; purity: 96%; UV/vis λ_{max} (in acetonitrile): 405 nm; IR (cm^{-1}): 1614 (C=O), 1450 (C=C).

4.2.16. (*E*)-1-(2-Hydroxy-6-methoxyphenyl)-3-(2,4,6-trimethoxyphenyl)prop-2-en-1-one (16)

Color: orange; mp 129–130 °C; Yield: 32%; purity: 89%; UV/vis λ_{max} (in acetonitrile): 385 nm; IR (cm^{-1}): 1613 (C=O), 1450 (C=C).

4.2.17. (*E*)-3-(3,5-Dimethoxyphenyl)-1-(2-hydroxy-5-methoxyphenyl)prop-2-en-1-one (17)

Color: orange; mp 82–83 °C; Yield: 23%; purity: 89%; UV/vis λ_{max} (in acetonitrile): 385 nm; IR (cm^{-1}): 1644 (C=O), 1454 (C=C).

4.2.18. (*E*)-1-(2-Hydroxy-5-methoxyphenyl)-3-(2,4,5-trimethoxyphenyl)prop-2-en-1-one (18)

Color: orange; mp 162–163 °C; Yield: 72%; purity: 91%; UV/vis λ_{max} (in acetonitrile): 415 nm; IR (cm^{-1}): 1640 (C=O), 1450 (C=C).

4.2.19. (*E*)-1-(2-Hydroxy-5-methoxyphenyl)-3-(2,4,6-trimethoxyphenyl)prop-2-en-1-one (19)

Color: orange; mp 169–170 °C; Yield: 48%; purity: 95%; UV/vis λ_{max} (in acetonitrile): 385 nm; IR (cm^{-1}): 1633 (C=O), 1462 (C=C).

4.2.20. (*E*)-1-(2-Hydroxy-5-methoxyphenyl)-3-(3-methoxyphenyl)prop-2-en-1-one (20)

Color: orange; mp 62–63 °C; Yield: 32%; purity: 98%; UV/vis λ_{max} (in acetonitrile): 350 nm; IR (cm^{-1}): 1642 (C=O), 1487 (C=C).

4.2.21. (*E*)-3-(2,3-Dimethoxyphenyl)-1-(2-hydroxy-5-methoxyphenyl)prop-2-en-1-one (21)

Color: orange; mp 102–103 °C; Yield: 94%; purity: 98%; UV/vis λ_{max} (in acetonitrile): 385 nm; IR (cm^{-1}): 1644 (C=O), 1469 (C=C).

4.2.22. (*E*)-3-(2,4-Dimethoxyphenyl)-1-(2-hydroxy-5-methoxyphenyl)prop-2-en-1-one (22)

Color: orange; mp 120–121 °C; Yield: 45%; purity: 99%; UV/vis λ_{max} (in acetonitrile): 385 nm; IR (cm^{-1}): 1640 (C=O), 1460 (C=C).

4.3. Preparation of chromene derivatives 23–26

All of the chromene derivatives (**23**–**26**) were synthesized as described in Scheme 1.[30] For the synthesis of chromene aldehydes **23**–**24**, K_2CO_3 (15 mmol) and acrolein (18 mmol) were added to a solution of methoxy salicylaldehyde (15 mmol) in dioxane (100 mL). The mixture was refluxed for 4 h and then poured into water (100 mL). The solution was extracted with chloroform (30 mL × 3). The combined organic layers were washed with water (30 mL × 2) successively. Next, the organic layer was dried over anhydrous $MgSO_4$. After the solvent was evaporated under vacuum, the residue was recrystallized from ethyl acetate/*n*-hexane to yield 2*H*-chromene-3-carbaldehyde as a yellow solid. The same reactions were performed between methoxy salicylaldehyde and methyl vinyl ketone to produce chromene ketones **25** and **26**. The physicochemical properties including color, melting point, yield, purity, UV/vis, IR, NMR, and HREIMS data for chromenes (**1**–**22**) are as follows.

4.3.1. 7-Methoxy-2*H*-chromene-3-carbaldehyde (23)

Color: brown; mp 84–85 °C (literature data 85–86 °C);[31] Yield: 22%; purity: 74%; UV/vis λ_{max} (in acetonitrile): 355 nm; IR (cm^{-1}): 1655 (C=O), 1270 (C=C); ^{1}H NMR (400 MHz, DMSO-d_6) δ 9.50 (s, 1H, O=C-H), 7.57 (s, 1H, H-4), 7.32 (d, 1H, H-5, J = 8.5 Hz), 6.61 (dd, 1H, H-6, J = 2.4, 8.5 Hz), 6.48 (d, 1H, H-8, J = 2.4 Hz), 4.92 (d, 1H, H-2, J = 1.1 Hz), 3.77 (s, 3H, 7-OCH_3); ^{13}C NMR (100 MHz, DMSO-d_6) δ 190.1 (C=O), 163.5 (C-7), 157.1 (C-9), 141.4 (C-4), 131.0 (C-5), 128.4 (C-3), 113.7 (C-10), 108.6 (C-6), 101.3 (C-8), 62.8 (C-2), 55.5 (7-OCH_3); HREIMS (*m*/*z*): Calcd for $C_{11}H_{10}O_3$ (M^+): 190.0630; Found 190.0631.

4.3.2. 6-Methoxy-2*H*-chromene-3-carbaldehyde (24)

Color: orange; mp 52–53 °C (literature data 51–52 °C);[31] Yield: 91%; purity: 90%; UV/vis λ_{max} (in acetonitrile): 385 nm; IR (cm^{-1}): 1666 (C=O), 1218 (C=C); ^{1}H NMR (400 MHz, DMSO-d_6) δ 9.59 (s, 1H, O=C-H), 7.59 (s, 1H, H-4), 7.01 (d, 1H, H-5, J = 3.0 Hz), 6.94 (dd, 1H, H-7, J = 3.0, 8.8 Hz), 6.84 (d, 1H, H-8, J = 8.8 Hz), 4.87 (d, 1H, H-2, J = 1.0 Hz), 3.74 (s, 3H, 6-OCH_3); ^{13}C NMR (100 MHz, DMSO-d_6) δ 190.6 (C=O), 154.0 (C-6), 149.2 (C-9), 141.1 (C-4), 132.0 (C-3), 121.1 (C-10), 119.0 (C-7), 116.8 (C-8), 113.5 (C-5), 62.4 (C-2), 55.5 (6-OCH_3); HREIMS (*m*/*z*): Calcd for $C_{11}H_{10}O_3$ (M^+): 190.0630; Found 190.0628.

4.3.3. 1-(6-Methoxy-2*H*-chromen-3-yl)ethanone (25)

Color: green; mp 56–57 °C (literature data 56–58 °C);[32] Yield: = 88%; purity: 99%; UV/vis λ_{max} (in acetonitrile): 375 nm; IR (cm^{-1}): 1638 (C=O), 1218 (C=C); ^{1}H NMR (400 MHz, DMSO-d_6) δ 7.65 (s, 1H, H-4), 6.97 (d, 1H, H-5, J = 3.0 Hz), 6.89 (dd, 1H, H-7, J = 3.0, 8.8 Hz), 6.81 (d, 1H, H-8, J = 8.8 Hz), 4.82 (d, 1H, H-2, J = 1.2 Hz), 3.72 (s, 3H, 6-OCH_3), 2.37 (s, 3H, O=C-CH_3); ^{13}C NMR (100 MHz, DMSO-d_6) δ 195.9 (C=O), 153.9 (C-6), 148.6 (C-9), 134.0 (C-4), 130.7 (C-3), 121.4 (C-10), 118.0 (C-7), 116.5 (C-8), 113.4 (C-5), 63.4 (C-2), 55.4 (6-OCH_3), 25.1 (O=C-CH_3); HREIMS (*m*/*z*): Calcd for $C_{12}H_{12}O_3$ (M^+): 204.0786; Found 204.0785.

4.3.4. 1-(7-Methoxy-2*H*-chromen-3-yl)ethanone (26)

Color: yellow; mp 81–82 °C; Yield: 56%; purity: 95%; UV/vis λ_{max} (in acetonitrile): 380 nm; IR (cm^{-1}): 1638 (C=O), 1208

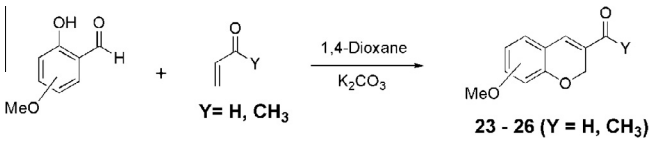

Scheme 1. The synthetic procedure for chromenes **23**–**26**.

(C=C); ^{1}H NMR (400 MHz, DMSO-d_6) δ 7.64 (s, 1H, H-4), 7.28 (d, 1H, H-5, J = 8.5 Hz), 6.59 (dd, 1H, H-6, J = 2.5, 8.5 Hz), 6.46 (d, 1H, H-8, J = 2.5 Hz), 4.87 (d, 1H, H-2, J = 1.1 Hz), 3.75 (s, 3H, 7-OCH_3), 2.34 (s, 3H, O=C-CH_3); ^{13}C NMR (100 MHz, DMSO-d_6) δ 190.9 (C=O), 162.8 (C-7), 156.4 (C-9), 134.2 (C-4), 130.7 (C-5), 127.0 (C-3), 113.8 (C-10), 108.3 (C-6), 101.2 (C-8), 63.7 (C-2), 55.4 (7-OCH_3), 24.9 (O=C-CH_3); HREIMS (m/z): Calcd for $C_{12}H_{12}O_3$ (M^+): 204.0786; Found 204.0786.

4.4. Quantitative structure–activity relationships (QSAR)

To obtain the 3D structures of the compounds used in these experiments, the structure of compound **6**, (*E*)-1-(2-hydroxyphenyl)-3-phenylprop-2-en-1-one, was first built using the sketch module provided by Sybyl 7.3 (Tripos, St. Louis, MO). Next, to find the most stable structure, a conformational search was performed using the grid search method of Sybyl. During the grid search, the selected bond was rotated from 0° to 360° in 15° increments. At each increment, the conformation was minimized using the Tripos force field and Gästeiger–Hückel charge. The maximum iteration for the minimization was set to 1000. The minimization process was terminated at the convergence criteria of the total energy (0.05 kcal/mol Å). Based on the structure of compound **6**, structures of the other 21 chalcones were modified, and their 3D structures were minimized. Similar to compound **6**, the 3D structure of compound **23**, 7-methyl-2*H*-chromene-3-carbaldehyde, was calculated using Sybyl 7.3. The 3D structures of the other three 2*H*-chromene-3-carbaldehydes were obtained using the 3D structure of compound **23** as a template. To perform CoMFA, the thermodynamic, conformational, electronic, and geometric descriptors were built and saved in a spreadsheet provided by the Sybyl program. For CoMFA, the aligned molecules were placed in a 3D cubic lattice with a grid spacing of 2.0 Å in the x, y, and z directions. A sp^3 hybridized carbon atom with a charge of +1 served as the probe atom to calculate steric and electrostatic fields. Their energy values were truncated to +30 kcal/mol. Likewise, for CoMSIA, same procedures were applied except additional descriptors such as H-bond acceptors, donors, and hydrophobic descriptors.[13]

4.5. Biological assay

4.5.1. Clonogenic assay

The biological data used for quantitative structure-activity relationships (QSAR) calculations was obtained from a clonogenic long-term survival assay in human cisplatin-resistant A2780/Cis ovarian cancer cells. A2780/Cis cells were counted and plated onto 24-well tissue culture plates (BD Falcon™; Becton Dickson Immunocytometry System) at a density of 5×10^3 cells/well in DMEM supplemented with 10% FBS. After attachment, the cells were treated with different concentrations of compounds (0, 5, 10, 20 μM) for 7 days. The cells were then fixed with 6% glutaraldehyde and stained with 0.1% crystal violet, as described previously.[33] The clonogenic survival densities were measured using the densitometry (MultiGuage, Fujifilm, Japan) and the half-maximal cell growth inhibitory concentration (GI_{50}) were obtained by SIGMAPLOT software (SYSTAT, Chicago, IL). A negative logarithmic scale of GI_{50} (pGI_{50}) was applied for the QSAR calculations.

4.5.2. Inhibition of cell growth

A2780/Cis cells were seeded into 96-well plates (2×10^3 cells/well) and treated with either vehicle (DMSO) or various concentrations of compound **16** or **19** (1–20 μM) for various times (0, 24, 48 h). The cell proliferation rate was assessed using a Cell Counting Kit-8™ (Dojindo Molecular Technologies, Gaithersburg, MD), according to the manufacturer's instructions.[13]

4.5.3. Flow cytometry analysis

A2780/Cis cells were treated with either vehicle (DMSO) or 20 μM compound **16** or **19** for 24 h, fixed in 70% ethanol, washed twice with phosphate-buffered saline, and stained with a 50 μg/mL propidium iodide solution, as described previously.[34] Cellular DNA content was analyzed using fluorescence-activated cell sorting (FACS) on a flow cytometer (FACSCalibur; Becton Dickinson Immunocytometry Systems, San Jose, CA).

4.5.4. Western blot analysis

A2780/Cis cells were treated with either vehicle (DMSO) or 20 μM compound **16** or **19**. At 24 h post-treatment, cells were collected and extracted in 20 mM HEPES (pH 7.2) containing 1% Triton X-100, 10% glycerol, 150 mM NaCl, 10 μg/mL leupeptin, and 1 mM phenylmethylsulfonyl fluoride. The protein samples (20 μg/lane) were then separated by 10% SDS–PAGE and transferred onto nitrocellulose filters, as described previously.[34] Western blotting was performed according to standard procedures using an antibody specific for PARP or cleaved caspase-7 (Asp198), purchased from Cell Signaling Technology (Beverly, MA). The antibody to glyceraldehyde phosphate dehydrogenase (GAPDH) from Santa Cruz Biotechnology (Santa Cruz, CA) was used as an internal control. The signals were developed using an enhanced chemiluminescence detection system (Amersham Pharmacia Biotech Inc., Piscataway, NJ).

4.5.5. Immunofluorescent microscopy

A2780/Cis cells plated on coverslips were treated with either vehicle (DMSO) or 20 μM compound **19**. After 24 h, the cells were fixed with 4% paraformaldehyde and permeabilized in 0.1% Triton X-100 and 2% bovine serum albumin, as described previously.[35] For microtubule staining, the samples were incubated with primary anti-α-tubulin antibody for 90 min and then with Alexa-Fluor 488-conjugated secondary antibody (Invitrogen, Carlsbad, CA) for 30 min. For detection of cleaved caspase-7, we used anti-cleaved caspase-7 (Asp198) antibody and Alexa-Fluor 555-conjugated secondary antibody (Invitrogen, Seoul, Korea). The nuclear DNA was stained with TO-PRO-3 iodide (Molecular Probes Inc., Eugene, OR). Stained cells were immediately observed under an EVOSf1® fluorescence microscope (Advance Microscopy Group, Bothell, WA).

4.6. In vitro inhibitory effect on aurora A kinase and their molecular binding mode

The kinase assay was performed using the EMD Millipore KinaseProfiler service assay protocol (EMD Millipore Corp., Billerica, MA).[36,37] The three dimensional (3D) structure of compound **16**, (*E*)-1-(2-hydroxy-6-methoxyphenyl)-3-(2,4,6-trimethoxyphenyl)prop-2-en-1-one, was determined by the X-ray crystallography. Recrystallization of compound **16** in ethanol gave orange colored crystals. The X-ray crystallography was performed with the help of the Korea Basic Science Institute at Jeonju and its detailed procedure followed the methods published previously.[38,39] The molecular structure of displacement ellipsoids drawn at the 50% probability level is shown in Figure S5 in Supplementary data contents. The 3D structure of aurA was adapted from the protein data bank (PDB). Of many crystallographic structures deposited in the PDB, 3o50.pdb originated from *Homo sapiens* was selected because of its high resolution (2.0 Å). It consists of a homodimeric structure, and the chain B contains more residues (126R–386K) than the chain A. As a result, 3o50B polymer chain was used for the docking experiments.[19] In silcio docking experiments were performed on an Intel Core 2 Quad Q6600 (2.4 GHz) Linux PC with Sybyl 7.3 (Tripos, St. Louis, MO).[40] To determine the binding site between aurA and compound **16**, 3o50B.pdb was analyzed using the LigPlot program. As shown in

Figure S6 in Supplementary data contents, a ligand, (*N*-{3-methyl-4-[(3-pyrimidin-4-ylpyridin-2-yl)oxy]phenyl}-3-(trifluoromethyl)benzamide, LJE) was embedded in 3o50B.pdb and 11 residues including Lys141, Gly142, Lys143, Val147, Lys162, Leu210, Lys258, Glu260, Asn261, Ala273, and Phe275 were found in the binding site. Before docking, the ligand LJE was deleted from 3o50B.pdb using the Sybyl program and apo-protein was obtained. Its solution structure was prepared using energy minimization. The root mean squared deviation (RMSD) between apo-protein and crystallographic structure was 0.6 Å. For the flexible docking procedure, the binding site determined by the LigPlot analysis was used. The docking process was iterated 30 times and 30 docking complexes were obtained. Based on the binding energy and docking image, the compound **16**–aurA complex was selected and used to elucidate the molecular binding mode. All 3D images were viewed using the PyMOL software (The PyMOL Molecular Graphics System, Version 1.0r1, Schrödinger, LLC).

Acknowledgements

This work was supported by the Priority Research Centers Program (NRF, 2009-0093824), Basic Science Research Program (NRF, 2013005214), and the next generation Biogreen21 program (RDA, PJ009532). S.Y. Shin was supported by the KU Research Professor Program of Konkuk University. S.Y. Shin and H. Jung contributed equally to this work.

Supplementary data

Supplementary data associated with this article can be found, in the online version, at http://dx.doi.org/10.1016/j.bmc.2014.01.058.

References and notes

1. Jemal, A.; Tiwari, R. C.; Murray, T.; Ghafoor, A.; Samuels, A.; Ward, E.; Feuer, E. J.; Thun, M. J. *CA Cancer J. Clin.* **2004**, *54*, 8.
2. Zhang, Y.; Wang, J.; Xiang, D.; Wang, D.; Xin, X. *Int. J. Oncol.* **2009**, *35*, 1069.
3. Piek, J. M.; van Diest, P. J.; Verheijen, R. H. *Adv. Exp. Med. Biol.* **2008**, *622*, 79.
4. Hu, X. W.; Meng, D.; Fang *J. Carcinog.* **2008**, *29*, 2369.
5. Luo, H.; Rankin, G. O.; Liu, L.; Daddysman, M. K.; Jiang, B. H.; Chen, Y. C. *Nutr. Cancer* **2009**, *61*, 554.
6. Xing, H.; Weng, D.; Chen, G.; Tao, W.; Zhu, T.; Yang, X.; Meng, L.; Wang, S.; Lu, Y.; Ma, D. *Cancer Lett.* **2008**, *261*, 108.
7. Arafa el, S. A.; Zhu, Q.; Barakat, B. M.; Wani, G.; Zhao, Q.; El-Mahdy, M. A.; Wani, A. A. *Cancer Res.* **2009**, *69*, 8910.
8. Deb Majumdar, I.; Devanabanda, A.; Fox, B.; Schwartzman, J.; Cong, H.; Porco, J. A., Jr.; Weber, H. C. *Biochem. Biophys. Res. Commun.* **2011**, *416*, 397.
9. Kamal, A.; Prabhakar, S.; Janaki Ramaiah, M.; Venkat Reddy, P.; Ratna Reddy, C.; Mallareddy, A.; Shankaraiah, N.; Lakshmi Narayan Reddy, T.; Pushpavalli, S. N.; Pal-Bhadra, M. *Eur. J. Med. Chem.* **2011**, *46*, 3820.
10. Kumar, V.; Kumar, S.; Hassan, M.; Wu, H.; Thimmulappa, R. K.; Kumar, A.; Sharma, S. K.; Parmar, V. S.; Biswal, S.; Malhotra, S. V. *J. Med. Chem.* **2011**, *54*, 4147.
11. Bazzaro, M.; Anchoori, R. K.; Mudiam, M. K.; Issaenko, O.; Kumar, S.; Karanam, B.; Lin, Z.; Isaksson Vogel, R.; Gavioli, R.; Destro, F.; Ferretti, V.; Roden, R. B.; Khan, S. R. *J. Med. Chem.* **2011**, *54*, 449.
12. Kamal, A.; Ramakrishna, G.; Raju, P.; Viswanath, A.; Ramaiah, M. J.; Balakishan, G.; Pal-Bhadra, M. *Bioorg. Med. Chem. Lett.* **2010**, *20*, 4865.
13. Shin, S. Y.; Woo, Y.; Hyun, J.; Yong, Y.; Koh, D.; Lee, Y. H.; Lim, Y. *Bioorg. Med. Chem. Lett.* **2011**, *21*, 6036.
14. Yalkinoglu, A. O.; Schlehofer, J. R.; Zur Hausen, H. *Int. J. Cancer* **1990**, *45*, 1195.
15. Pirhadi, S.; Ghasemi, J. B. *Eur. J. Med. Chem.* **2010**, *45*, 4897.
16. Lazebnik, Y. A.; Kaufmann, S. H.; Desnoyers, S.; Poirier, G. G.; Earnshaw, W. C. *Nature* **1994**, *371*, 346.
17. Carmena, M.; Earnshaw, W. C. *Nat. Rev. Mol. Cell Biol.* **2003**, *4*, 842.
18. Nikonova, A. S.; Astsaturov, I.; Serebriiskii, I. G.; Dunbrack, R. L., Jr.; Golemis, E. A. *Cell. Mol. Life Sci.* **2013**, *70*, 661.
19. Cee, V. J.; Schenkel, L. B.; Hodous, B. L.; Deak, H. L.; Nguyen, H. N.; Olivieri, P. R.; Romero, K.; Bak, A.; Be, X.; Bellon, S.; Bush, T. L.; Cheng, A. C.; Chung, G.; Coats, S.; Eden, P. M.; Hanestad, K.; Gallant, P. L.; Gu, Y.; Huang, X.; Kendall, R. L.; Lin, M. H.; Morrison, M. J.; Patel, V. F.; Radinsky, R.; Rose, P. E.; Ross, S.; Sun, J. R.; Tang, J.; Zhao, H.; Payton, M.; Geuns-Meyer, S. D. *J. Med. Chem.* **2010**, *53*, 6368.
20. Wallace, A. C.; Laskowski, R. A.; Thornton, J. M. *Protein Eng.* **1995**, *8*, 127.
21. Yong, Y.; Ahn, S.; Hwang, D.; Yoon, H.; Jo, G.; Kim, Y. H.; Kim, S. H.; Koh, D.; Lim, Y. *Magn. Reson. Chem.* **2013**, *51*, 364.
22. Goddard, T. D.; Kneller, D. G. Sparky 3, University of California: San Francisco 2008. http://www.cgl.ucsf.edu/home/sparky/.
23. Detsi, A.; Majdalani, M.; Kontogiorgis, C. A.; Hadjipavlou-Litina, D.; Kefalas, P. *Bioorg. Med. Chem.* **2009**, *17*, 8073.
24. Alcantara, A. R.; Marinas, J. M.; Sinisterra, J. V. *Tetrahedron Lett.* **1987**, *28*, 1515.
25. Nielsen, S. F.; Christensen, S. B.; Cruciani, G.; Kharazmi, A.; Liljefors, T. *J. Med. Chem.* **1998**, *41*, 4819.
26. Begum, N. A.; Roy, N.; Laskar, R. A.; Roy, K. *Med. Chem. Res.* **2010**, *20*, 184.
27. Fun, H. K.; Suwunwong, T.; Chanawanno, K.; Wisitsak, P.; Chantrapromma, S. *Acta Crystallogr. Sect. E* **2011**, *67*, o2287.
28. Takahashi, H.; Kubota, Y.; Fang, L.; Onda, M. *Heterocycles* **1986**, *24*, 1099.
29. Bargellini, G.; Peratoner, E. *Gazz. Chim.* **1919**, *49*, 64.
30. Nazarian, Z.; Emami, S.; Heydari, S.; Ardestani, S. K.; Nakhjiri, M.; Poorrajab, F.; Shafiee, A.; Foroumadi, A. *Eur. J. Med. Chem.* **2010**, *45*, 1424.
31. Zhang, J.; Lou, C.; Hu, Z.; Yan, M. *Arkivoc* **2009**, *16*, 362.
32. Sorkhi, M.; Forouzani, M.; Dehgan, G.; Abdollahi, M.; Shafiee, A.; Foroumadi, A. *Asian J. Chem.* **2008**, *20*, 2151.
33. Franken, N. A.; Rodermond, H. M.; Stap, J.; Haveman, J.; van Bree, C. *Nat. Protoc.* **2006**, *1*, 2315.
34. Shin, S. Y.; Yong, Y.; Kim, C. G.; Lee, Y. H.; Lim, Y. *Cancer Lett.* **2010**, *287*, 231.
35. Shin, S. Y.; Bahk, Y. Y.; Ko, J.; Chung, I. Y.; Lee, Y. S.; Downward, J.; Eibel, H.; Sharma, P. M.; Olefsky, J. M.; Kim, Y. H.; Lee, B.; Lee, Y. H. *EMBO J.* **2006**, *25*, 1093.
36. Sharma, S. K.; Kumar, P.; Narasimhan, B.; Ramasamy, K.; Mani, V.; Mishra, R. K.; Majeed, A. B. *Eur. J. Med. Chem.* **2012**, *48*, 16.
37. Shin, S. Y.; Yoon, H.; Hwang, D.; Ahn, S.; Kim, D. W.; Koh, D.; Lee, Y. H.; Lim, Y. *Bioorg. Med. Chem.* **2013**, *21*, 7018.
38. Shin, S. Y.; Yoon, H.; Ahn, S.; Kim, D. W.; Kim, S. H.; Koh, D.; Lee, Y. H.; Lim, Y. *Bioorg. Med. Chem.* **2013**, *21*, 4250.
39. Lim, Y.; Koh, D. *Acta Crystallogr. Sect. E* **2013**, *69*, o514.
40. Lee, S.; Jo, G.; Hwang, D.; Woo, Y.; Lee, Y.; Yong, Y.; Kang, K.; Hyun, J.; Kim, Y. K.; Kim, D. W.; Lim, Y. *J. Korean Soc. Appl. Biol. Chem.* **2011**, *54*, 633.